applied sciences

Article

Sep-RefineNet: A Deinterleaving Method for Radar Signals Based on Semantic Segmentation

Yongjiang Mao [1,2,3], Wenjuan Ren [1,2,*], Xipeng Li [4], Zhanpeng Yang [1,2] and Wei Cao [1,2]

1 Key Laboratory of Network Information System Technology, Institute of Electronics, Chinese Academy of Sciences, Beijing 100190, China
2 Aerospace Information Research Institute, Chinese Academy of Sciences, Beijing 100190, China
3 University of Chinese Academy of Sciences, Beijing 100049, China
4 Systems Engineering Institute, Beijing 100080, China
* Correspondence: renwj@aircas.ac.cn; Tel.: +86-134-6672-1075

Abstract: With the progress of signal processing technology and the emergence of new system radars, the space electromagnetic environment becomes more and more complex, which puts forward higher requirements for the deinterleaving method of radar signals. Traditional signal deinterleaving algorithms rely heavily on manual experience threshold and have poor robustness. To address this problem, we designed an intelligent radar signal deinterleaving algorithm that was completed by encoding the frequency characteristic matrix and semantic segmentation network, named Sep-RefineNet. The frequency characteristic matrix can well construct the semantic features of different pulse streams of radar signals. The Sep-RefineNet semantic segmentation network can complete pixel-level segmentation of the frequency characteristic matrix and finally uses position decoding and verification to obtain the position in the original pulse stream to complete radar signals deinterleaving. The proposed method avoids the processing of threshold judgment and pulse sequence search in traditional methods. The results of the experiment show that this algorithm improves the deinterleaving accuracy and has a good against-noise ability of aliasing pulses and missing pulses.

Keywords: radar signals deinterleaving; frequency characteristic matrix; semantic segmentation; Sep-RefineNet

check for updates

Citation: Mao, Y.; Ren, W.; Li, X.; Yang, Z.; Cao, W. Sep-RefineNet: A Deinterleaving Method for Radar Signals Based on Semantic Segmentation. *Appl. Sci.* **2023**, *13*, 2726. https://doi.org/10.3390/app13042726

Academic Editor: Gordana Jovanovic Dolecek

Received: 1 February 2023
Revised: 14 February 2023
Accepted: 15 February 2023
Published: 20 February 2023

Copyright: © 2023 by the authors. Licensee MDPI, Basel, Switzerland. This article is an open access article distributed under the terms and conditions of the Creative Commons Attribution (CC BY) license (https://creativecommons.org/licenses/by/4.0/).

1. Introduction

In modern warfare, electronic warfare is a very important field [1]. Scientists and technologists from various countries pay great attention to the application and development of electronic technology, hoping to gain control of the space electromagnetic spectrum through the advantages of electronic countermeasures, to win the victory of electronic warfare [2,3]. The pulse streams deinterleaving of radar signals are the basic part of electronic countermeasures [4]. The definition of deinterleaving is to separate the aliased pulse signals received in space. However, the complex space electromagnetic environment and the application of low-interception radar make it difficult for traditional deinterleaving algorithms to deal with complex situations such as aliasing pulses and missing pulses [5,6].

For the traditional signal deinterleaving algorithms, there are some disadvantages as follows. First, a lot of prior knowledge is required. For example, in the 1970s and 1980s, the space electromagnetic environment was relatively simple, and the types of radar emitter were fixed, and thus, the template matching method was proposed [7]. There is a need to establish a characteristic database of radar emitter in advance and compare the pulse description words (PDW) of received signals with the database to complete the signal deinterleaving. In [8], a pulse repetition interval (PRI) heuristic search method was proposed. By looking for the difference between the first pulse and the following pulses, it was judged whether the difference between the initial time of arrival (TOA) and the *i*-th TOA is in an appropriate interval to complete the deinterleaving. In [9], the pulse end time needed to be estimated in advance before PRI transformation, which is not practical. The traditional histogram method needs to adjust the threshold judgment parameters for different data in order to estimate the potential PRI, which relies on manual experience heavily. However, in most cases, the electronic support measure (ESM) [10] intercepts non-cooperative signals, and it is difficult to estimate the threshold in advance. Some scholars also proposed the method of plane transformation [11], which transforms the pulse signal into a two-dimensional plane for sorting. These methods are seriously disturbed by manual empirical parameters, and the effect on jittered and staggered PRI is not ideal. When aliasing pulses and missing pulses occur, the deinterleaving ability of these methods will be greatly reduced, and they cannot be applied to the current and future complex space electromagnetic environment and emerging new system radars.

In this paper, in the case of aliasing pulses and missing pulses, the semantic features of different PRI are extracted by deep learning, the influence of manual experience parameters is reduced, the anti-noise ability of the algorithm is improved, and the deinterleaving of radar signals is completed intelligently. We propose a frequency characteristic matrix (FCM) to encode PRI, combined with a semantic segmentation network named Sep-RefineNet to identify the PRI features, and finally complete the radar signals deinterleaving by position decoding. The proposed method has an ability to oppose aliasing pulses and missing pulses. It solves the problem that traditional algorithms rely too much on manual experience parameters, and has better robustness for sorting different modulation types of PRI. The proposed method can effectively deinterleave constant PRI, jittered PRI, and staggered PRI within 20% of aliasing pulses and missing pulses, respectively. When the aliasing pulses and missing pulses are both 10%, this method's F1-score is 0.931, which is better than traditional deinterleaving algorithms.

Our major contributions are summarized as follows:

- An FCM is designed to encode and decode the PRI of radar pulse signals. It encodes different PRI's semantic information into the FCM.
- A multi-receptive field and multi-channel separation semantic segmentation network named Sep-RefineNet is used to learn the semantic features of the FCM. Through position decoding, the deinterleaving algorithm is made more intelligent, reducing the dependence on manual experience parameters.
- Under the influence of aliasing pluses and missing pluses, it can sort constant PRI, staggered PRI, and jittered PRI, and improve the robustness and accuracy of the deinterleaving.

Section 2 of this paper introduces the related work about radar signals deinterleaving. Section 3 introduces the deinterleaving system framework. It includes the methods of encoding and position decoding of the FCM and the semantic segmentation network named Sep-RefineNet. Experimental data and results are given in Section 4, which also analyzes the effectiveness of the proposed method. Finally, the work of this paper is summarized in Section 5.

2. Related Work

The purpose of radar signals deinterleaving is to separate the received pulse stream according to each radar emitter, which is shown in Figure 1.

Deinterleaving generally uses the following PDW, such as TOA, direction of arrival, pulse width, radio frequency, and pulse amplitude. Normally, signal deinterleaving is divided into two steps. One is to dilute the pulse stream density through pre-sorting, and the other is to complete the main sorting through TOA sequence [12]. The parameter for the main sorting is PRI, which is the difference between the TOA of two adjacent pulses of the same radar emitter. Its mathematical model is $PRI = TOA_{i+1} - TOA_i$. Radar with different working modes and systems may have different PRI modulation modes, such as constant PRI, jittered PRI, and staggered PRI. The constant PRI is considered to be fixed in two adjacent pulses of the radar emitter under ideal conditions. In practice, it generally does not exceed 1% of the central value. The jittered PRI is centered on a value PRI_c and changes within the range of this value. The mathematical model is $PRI = PRI_c + \sigma_i$, where $\sigma_i \in [-\varepsilon, \varepsilon]$, ε is the amount of jitter, the jitter rate is δ, and the general jitter rate is $\delta \in [5\%, 30\%]$. The staggered PRI means there are two or more fixed PRI_i values in a radar emitter, and each PRI_i is called its sub-period.

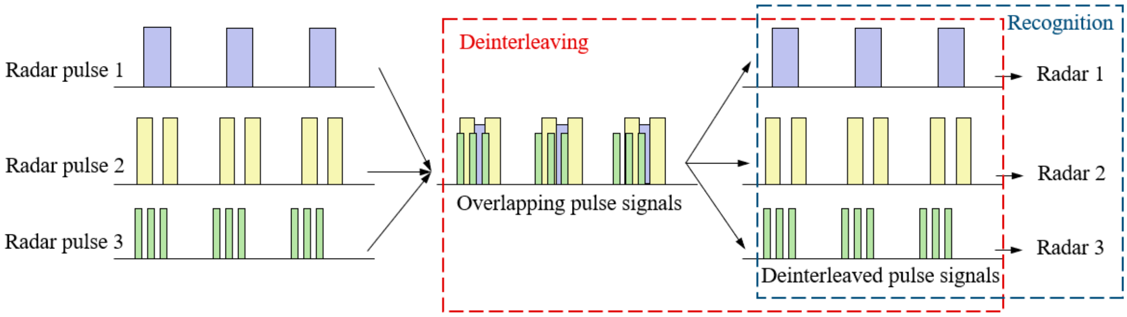

Figure 1. Radar pulse signals deinterleaving.

In the last few decades, many scholars have made contributions in the field of radar signal deinterleaving. They proposed many classical algorithms to make the deinterleaving system more robust, accurate and intelligent. They are pushing forward the field of radar signal deinterleaving.

In the 1970s, Saperstein [7] proposed a template-matching method based on the actual space electromagnetic situation. First, the database of the main characteristic parameters of the radar emitter is established in advance, and then, the PDW of the received pulse signal is measured and compared with the database. This method achieved a good sorting effect when the electromagnetic environment was simple and the radar modulation modes were relatively fixed. In [8], the method of impulse heuristic search was proposed. First, assuming the base TOA and reference TOA in a pulse stream, the difference between the two pulses is obtained. After considering the actual error, it is judged whether the pulse difference is within the allowable error range to complete the deinterleaving. This method requires a lot of prior knowledge. To have a high search accuracy, the key is how to accurately find the potential PRI from the pulse stream. Some scholars have conducted a lot of work on this issue, mainly focusing on the method of PRI histogram. The cumulative difference histogram (CDIF) proposed in [13] and the sequential difference histogram (SDIF) proposed in [14] are representative of histogram methods. CDIF is an improvement of the traditional histogram method. It combines the traditional histogram with sequence search to suppress the generation of harmonics, but it needs to accumulate the statistical difference histograms, which require a large amount of calculations. CDIF has a threshold judgment before pulse search, and the threshold function is Equation (1).

$$f_{CDIF}(\tau) = k \times \left(\frac{T}{\tau}\right) \tag{1}$$

where T is the sampling time, and k is an adjustable parameter. Generally, $k < 1$, and τ is the repetition interval. SDIF is an improvement of CDIF. The SDIF algorithm no longer accumulates the histogram, but directly compares the difference of the TOA sequence with the set threshold, which improves the efficiency of the deinterleaving algorithm. After the SDIF algorithm was proposed, it was widely used in the engineering of radar emitter signal deinterleaving. Equation (2) is the threshold function of the SDIF.

$$f_{SDIF}(\tau) = k \times (E - C)e^{\frac{-\tau}{\alpha N}} \tag{2}$$

where $\alpha \in [0, 1]$ is an adjustable parameter, N is the number of histogram intervals, C is the histogram order, E is the number of pulses, and k is a constant set base on experience. In [15], the SDIF deinterleaving was improved, through the clustering algorithm to deal with the difference of random distribution, and it is combined with the PRI transformation after the potential PRI exceeds the threshold, the harmonics can be further suppressed, and the estimated PRI accuracy can be improved. When the aliasing pulse is 16% and the missing pulse is 20%, the deinterleaving is complete, but the accuracy is not high. In [16], the overlapped PRI bins are introduced to sort different PRI modulation modes, and the phase factor is introduced into the autocorrelation function, which can effectively suppress harmonics and resist noise. In Equation (3), the PRI transformation first regards the radar pulse sequence as the sum of a series of unit impulse responses, where N is the number of pulse sequences. Then, Equation (4) is obtained by the autocorrelation function of Equation (3), and the pulse sequence is used in PRI transformation to obtain Equation (5). where $\tau > 0$, and j is the imaginary number unit. Substitute Equation (3) into Equation (5) to obtain Equation (6).

$$g(t) = \sum_{n=0}^{N-1} \delta(t - t_n) \tag{3}$$

$$G(\tau) = \int_{-\infty}^{\infty} g(t)g(t+\tau)d\tau \tag{4}$$

$$D(\tau) = \int_{-\infty}^{\infty} g(t)g(t+\tau)e^{\frac{2\pi jt}{\tau}}d\tau \tag{5}$$

$$D(\tau) = \sum_{n=1}^{N-1} \sum_{m=0}^{n-1} \delta(\tau - t_n + t_m)e^{\left[\frac{2\pi jt}{t_n - t_m}\right]} \tag{6}$$

where $|D(\tau)|$ is the spectral function of the pulsed PRI. The peak value in this spectral function is the estimated potential PRI. $e^{\frac{2\pi jt}{\tau}}$ is the introduced phase factor, which can suppress the harmonics generated by PRI transformation and estimate the value of PRI accurately. When estimating potential PRI, the pulse current density, sub-harmonic elimination, and noise elimination rules are considered to adapt to the pulse signal [17]. The traditional PRI transformation cannot effectively deinterleave the staggered PRI, which has limitations. In [18], through the improved machine learning clustering method, combined with PDW parameters such as pulse width and radio frequency, the pre-sorting is completed, which can help the main sorting to dilute the pulse stream. However, for example, K-means is difficult to estimate the number of clusters K in advance, and the cluster radius of DBSCAN also requires strong prior knowledge of the intercepted signals, which is not practical.

In recent years, some scholars have also used deep learning methods to complete signal deinterleaving. In [19,20], the time–frequency analysis method and convolutional neural network are used for recognition of the signal's intra-pulse modulation characteristics and complete signal deinterleaving task in a specific situation, opening up a new research direction. In [21], the received pulse stream is first sorted by the traditional histogram method, and then, the processed pulse sequence is fed to long short-term memory (LSTM) for training. Through the learning of the existing sequence, a model that can predict the same distribution of pulses is trained to predict the next arriving pulse. This method has a high dependence on the traditional deinterleaving algorithm. Ref. [22] combines a recurrent neural network and attention module to complete the identification of different PRI modulation modes, but did not complete the deinterleaving task. Deep learning has many advantages, and it has a good performance in object detection, recognition, and semantic segmentation. Using deep learning to complete the deinterleaving of radar emitter signals and extracting signal features through neural networks can improve the anti-noise ability and reduce manual participation in the signal deinterleaving. The trained model does not need to set empirical parameters again, and the model has high robustness. However, there are still few studies using deep learning to complete radar signal deinterleaving.

Many radar signal deinterleaving systems have been designed, but under the interference of noise such as aliasing pulses, missing pulses, and measurement error, it is still a challenging problem to improve the accuracy and reduce the dependence on manual experience to complete the radar signal deinterleaving.

3. System Framework and Method

An intelligent algorithm is designed to complete radar signals deinterleaving with high accuracy. The first step is to extract the TOA sequence of the radar signals, make a self-correlation difference of the TOA sequence to obtain the PRI transformation matrix, and count the frequency of potential PRI to obtain the FCM. Then, normalize the elements in the FCM and feed them to the network of Sep-RefineNet for model training. Finally, the position of the prediction results is decoded to obtain that each pulse belongs to its own radar emitter, and the signal interleaving is completed. The system framework is shown in Figure 2.

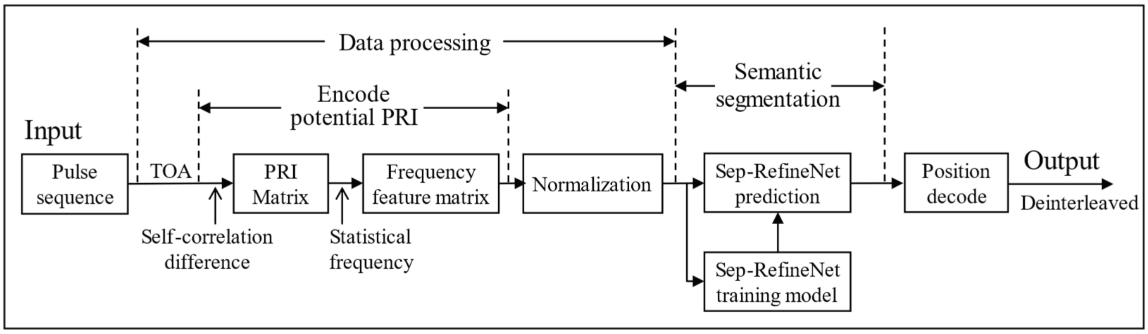

Figure 2. The system framework of radar signals deinterleaving.

The one-dimensional pulse sequence is transformed into a two-dimensional matrix through the coding of FCM, and the FCM can extract the PRI features of pulse streams. The semantic segmentation network named Sep-RefineNet can better identify the contextual semantic features of FCM and finally complete pixel-level segmentation and position decoding. The proposed method can accurately complete the task of the deinterleaving radar signals in the interference of noise.

3.1. Frequency Characteristic Matrix

The frequency characteristic matrix (FCM) is a method we propose to encode the PRI of pulse streams. This method avoids the threshold judgment and pulse sequence search process of the traditional deinterleaving algorithm and reduces the manual participation in the sorting. The situation that all the pulses of radar emitter are missed due to a potential PRI not exceeding the threshold is prevented.

The encoding method of FCM is presented as follows. First, the TOA in PDW is extracted, and the obtained TOA sequence is divided into a TOA vector with a length of 512 and a width of 1. Then, the TOA vector is subjected to a 10-order self-correlation difference to obtain the PRI transformation matrix (TM). The value of the $TM_{(i,j)}$ is the j-th pulse minus the i-th pulse of the TOA vector. Count the frequency of potential PRI in the TM. Considering the measurement error of TOA, the allowable error in statistics is 10 μs. Finally, the frequency of different potential PRI is written into the corresponding FCM to complete the feature encoding of the pulse stream. Before feeding it to Sep-RefineNet to learn the FCM features, it needs to be standardized. The standardized value of FCM is shown in Equation (7).

$$f_{(i,j)} = 255 \times \left[\frac{FCM_{(i,j)} - min(FCM)}{max(FCM) - min(FCM)} \right] \quad (7)$$

Mapping the feature elements of FCM to [0, 255], the maximum value is 255, and the minimum value is 0, which can better help the neural network learn the semantic feature of PRI. When the length of the pulse stream is less than 512, the subsequent position is filled with zeros. The encoding process of the FCM is presented in Figure 3.

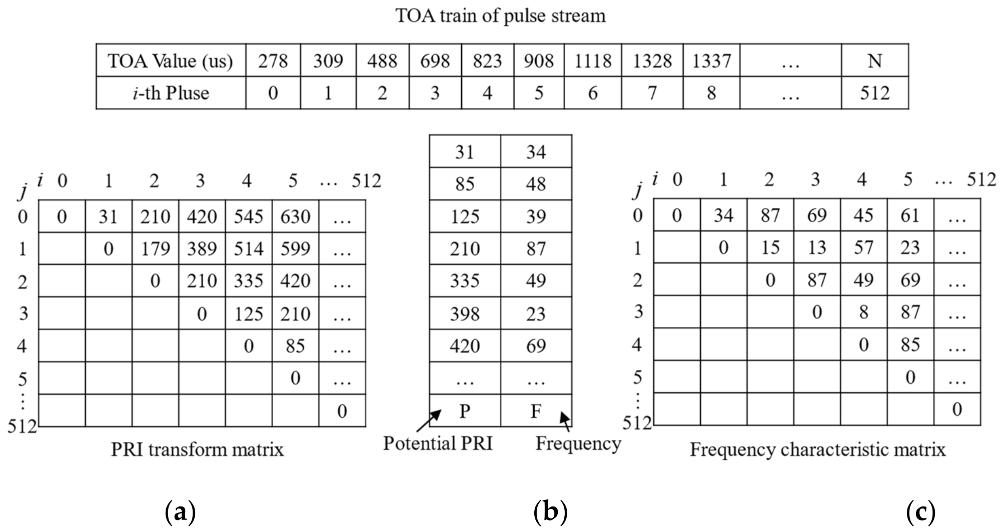

Figure 3. Encoding process of FCM: (**a**) PRI transformation matrix obtained by the self-correlation difference of the TOA sequence; (**b**) the statistical potential PRI; (**c**) generated frequency characteristic matrix.

After obtaining the FCM constructed by the potential PRI, the paired label matrix is obtained in Figure 4.

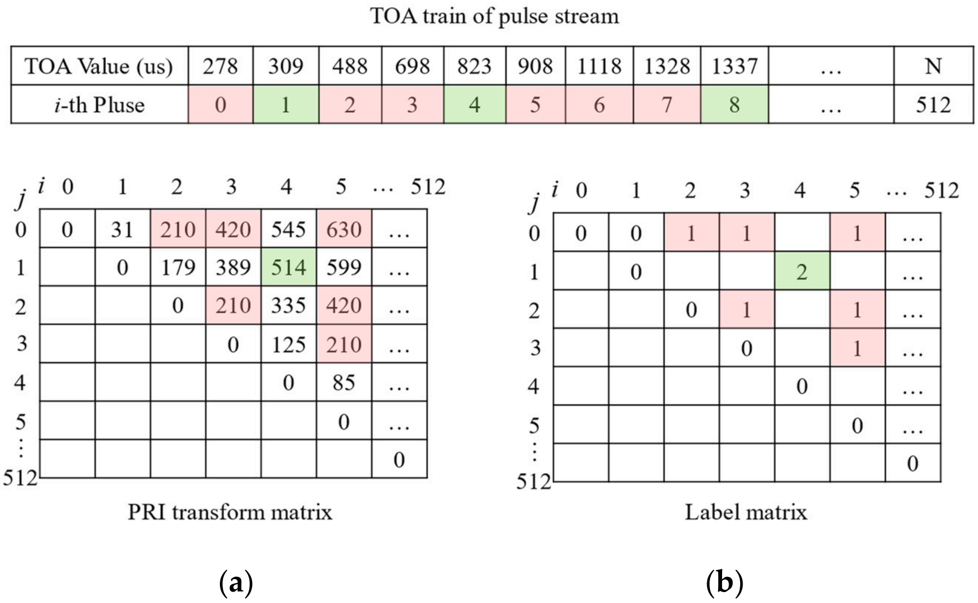

Figure 4. The result of label matrix: (**a**) PRI transform matrix; (**b**) generated label matrix.

According to the corresponding position of the pulse in the pulse streams, the category label of the radar emitter to which it belongs can be marked, and the paired FCM and label matrix can be obtained. During the experiment, in order to add a verification step when decoding the position, the FCM and label matrix are both symmetrical about the diagonal. After the FCM is symmetric, the PRI of the radar emitter has clearer semantic features of texture and structure. After the label matrix is symmetric, it can be compared whether the label at the symmetrical position is correct, so as to verify the post-processing algorithm of deinterleaving. The visualization of the FCM and label matrix is presented in Figure 5.

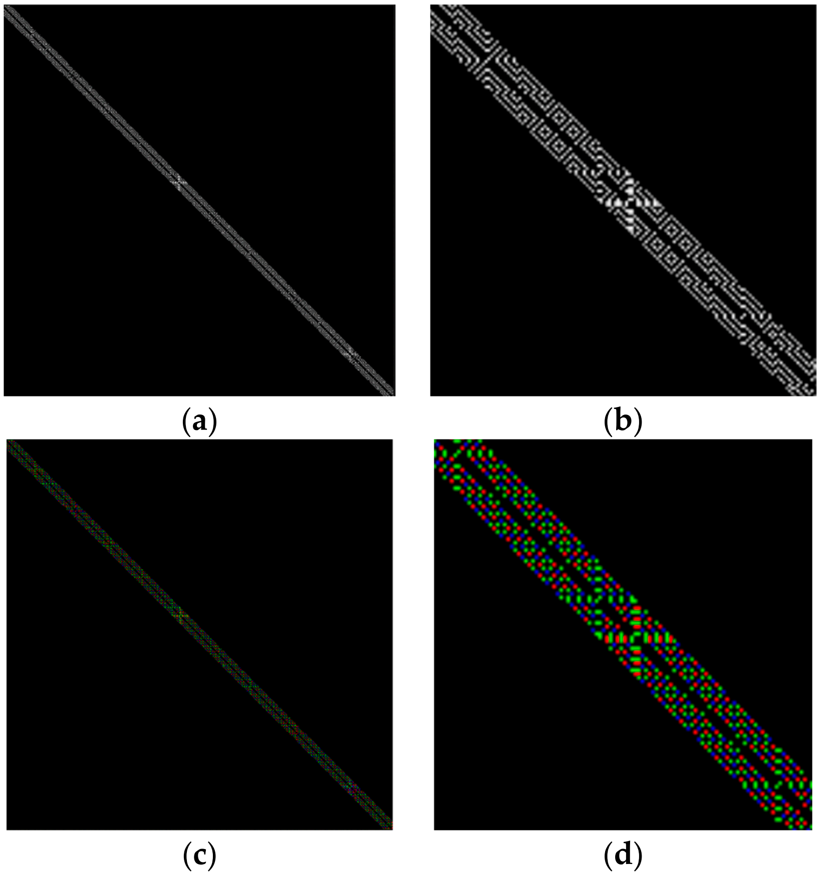

Figure 5. Visualization image of FCM and label matrix: (**a**) encoded FCM visualization image; (**b**) partial enlargement of the FCM; (**c**) visualization image of the corresponding label matrix; (**d**) partial enlargement of the label matrix.

The position decoding method of the FCM is as follows. First, the label of each element in the prediction matrix is obtained, and then, the elements with different predicate results in symmetrical positions are eliminated to ensure the accuracy of deinterleaving. Obtain the symmetric position of the same label in the prediction matrix, and select the coordinates of the original TOA pulse stream as a set; then, the set of radar pulse sequences with the same label can be obtained, and complete the signal deinterleaving. This method encodes and decodes the received pulse stream to complete the deinterleaving of radar signals, avoiding the dependence of traditional methods on threshold judgment and pulse sequence search, and relies on the FCM to reflect the characteristics of different PRI in the position and between elements for the texture and structural features. Finally, combined with Sep-RefineNet to segment the pixel-level semantic features of FCM, the deinterleaving of radar signals is intelligently completed.

3.2. Sep-RefineNet

Feed the encoded FCM and paired label matrix to a separable refinement network (Sep-RefineNet) to extract semantic features. The definition of semantics is the characteristic relationship between the elements formed by the PRI of the pulse sequence in the FCM. It includes texture, shape, and structure formed by different PRI modulation modes, aliasing pulses, and missing pulses. The context information of the pulse sequence represents that each FCM element is not isolated but has a semantic relationship with the surrounding elements and potential PRI, which determines the texture, shape, and structural features presented.

As the depth of the network increases, problems such as loss of feature information, gradient vanishing, and gradient explosion will inevitably occur in traditional deep learning networks. It makes the deep semantic information of FCM difficult to extract. We designed the Sep-Residual unit with channel separation and multi-receptive fields, multi-resolution fusion, and chained residual pooling, and built a deep learning network that can fuse shallow and deep semantic information. Identify and segment the FCM to complete the radar signal deinterleaving. The designed Sep-RefineNet is presented in Figure 6.

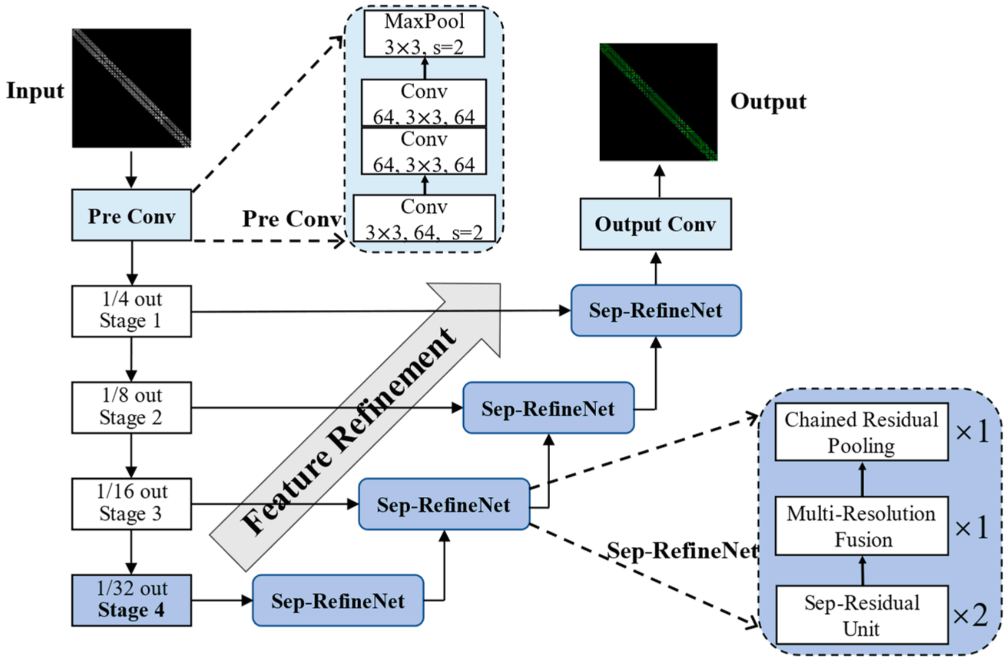

Figure 6. The network structure of Sep-RefineNet.

First, the FCM is input. The Pre Conv block is three 3×3 convolutional layers and a pooling layer. The step size of the first convolutional layer is two, which adjusts the feature map size, and the next two consecutive convolutional layers have a step size of 1, which is used to extract features. The max pooling layer resizes the feature map and outputs the largest feature element. The backbone is ResNet50 [23], which is used to extract the features of FCM. It outputs four stages on different resolutions, which are 1/4, 1/8, 1/16, and 1/32 the size of the original resolution. Then, these four stages will pass through a Sep-RefineNet block, and the output of the fourth stage will complete the Sep-Residual unit with the output of the third Stage. Then, multi-resolution fusion and chained residual pooling are used for feature fusion. The output of the third stage will also extract features through the same Sep-RefineNet as the output of the second stage. By analogy, the output to the last Sep-RefineNet block is the input of the Output Conv. The Output Conv is three concatenated convolutional layers: the first two layers are used for feature extraction and channel number adjustment, and the last layer is used to map to the predicted label of FCM. The deep feature layer has more information such as the texture and structure of the FCM, and the shallow feature layer has more edge and detail information. Sep-RefineNet has good capabilities for FCM feature extraction, feature fusion and semantic segmentation. Figure 7 is the Sep-Residual unit.

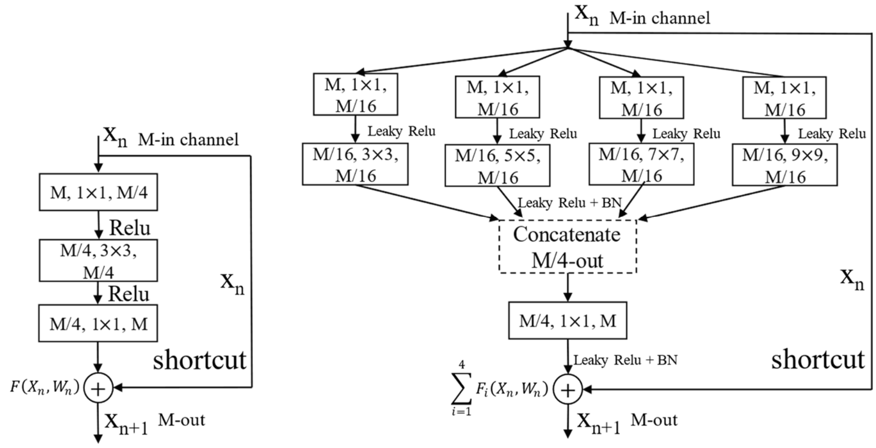

(**a**) (**b**)

Figure 7. Schematic diagram of the Sep-Residual unit: (**a**) original ResNet50 residual block [23]; (**b**) improved Sep-Residual unit; (**b**) multiple channels and multiple receptive fields, which can better extract the characteristics of the signal.

The three parameters of the rectangular box in Figure 7 are channel of input, kernel size of convolution, and channel of output. The number of input channels is M, and the features extracted by the Sep-Residual unit are added to obtain the output. In the Sep-residual unit, the first layer uses a convolution kernel size with 1×1, adjusts the number of channels, and obtains the M/16 output channels. Leaky ReLu: $x = max\{0.01x, x\}$ is an activation function to improve the nonlinear ability of network fitting. Then, the receptive fields of different sizes are obtained, which are 3, 5, 7, and 9, respectively. It can enrich the extraction characteristics of the encoding FCM. Then, concatenate the four branches with M/16 channels to obtain M/4 feature maps. Finally, use the convolution kernel of 1×1 to adjust the number of channels, and add them with the M feature maps before convolution through shortcut to obtain the residual output. Batch normalization layer is used to complete a batch of input data to the same distribution data with average value of 0 and variance value of 1 [24]. It can help the network to converge faster and reduce the over-fitting. The output of Sep-Residual unit is X_{n+1} in Equation (8).

$$X_{n+1} = X_n + \sum_{i=1}^{4} F_i(X_n, W_n) \tag{8}$$

where $F_i(X_n, W_n)$ is convolution result of X_n in i-th channel. Sep-Residual unit will better obtain the characteristics of FCM in the case of aliasing pulses and missing pulses, with multiple scales and multiple receptive fields. After being processed by the Sep-Residual unit, it needs to pass the Multi-resolution Fusion, and its structure is shown in Figure 8a.

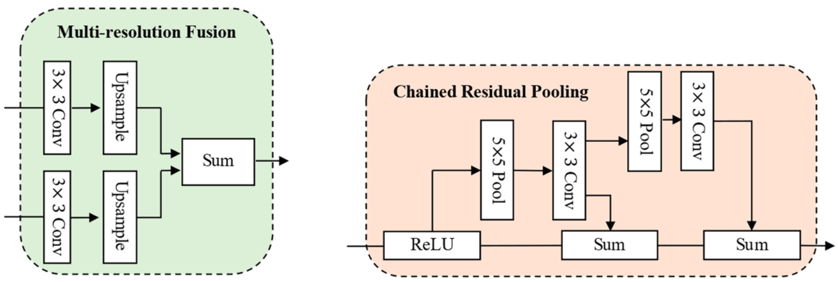

(**a**) (**b**)

Figure 8. Schematic diagram of the unit structure: (**a**) Multi-resolution Fusion; (**b**) Chained Residual Pooling [25].

The Multi-resolution Fusion fuses the output of the two Sep-Residual units. Through the 3×3 convolutional layer, the features of the deep stage need to be upsampled and then added to the features of the shallow stage. In this way, deep semantic information can be obtained without losing shallow texture and edge information. The output of Multi-resolution Fusion is the input of Chained Residual Pooling. Through the activation function ReLU and the 5×5 large pooling kernel on the branch, the attention to the large structural features in FCM is improved. Initial learning rate (LR) sets $LR = 1 \times 10^{-4}$, and then, the learning rate of every 20 epochs is reduced to 1/2 of the original until it drops to 10^{-5}. The updated method of the learning rate is Equation (9).

$$LR = max(lr_{initial} \times 0.5^{\lfloor epoch/20 \rfloor}, 10^{-5}) \tag{9}$$

In the 100 epochs, the learning rate continues to decline to better complete the training of the model. Considering that labels will be interfered with by noise in the actual situation, label smoothing [26] is introduced, which can prevent the model from over-fitting the label in Equation (10).

$$y' = (1 - \varepsilon) \times y + \frac{\varepsilon}{K} \tag{10}$$

where y is original hard label, y' is smoothing label, $\varepsilon = 0.1$ is the acceptable error rate, and $K = 5$ is the number of classifications. The hard label only has 0 or 1. The smoothing label has an acceptable error, reduces the method over-fitting, and makes the signal deinterleaving system have the ability to oppose interference. Due to signal characteristics encoding into FCM, it is determined that the positive and negative samples will have a serious imbalance. Therefore, the loss function in this experiment is the focal loss [27]. Substituting Equation (10) into the focal loss, Equation (11) is obtained.

$$focal\ loss = -\sum_{i=0}^{n} \left[\alpha(1-p) \times y' logp + (1-\alpha)p^{\gamma} \times \left(1 - y'\right) log(1-p)\right] \tag{11}$$

The weight coefficient $\alpha = 0.9$ is introduced to adjust the proportion of the positive and negative samples, and the tunable focusing parameter $\gamma = 2$ is used to control the contribution of the difficulty of sample classification to the loss function. Since the number of negative samples is more than the positive samples, if the contribution of negative samples is not suppressed, the contribution will be much higher than the positive samples, which will lead to the poor fitting ability of the model to positive samples. The focal loss can solve this problem, suppress the contribution of negative samples, and pay more attention to samples that are difficult to distinguish and misclassify. The experimental results show that the improved focal loss is better than cross-entropy for the Sep-RefineNet to identify FCM. Finally, each layer's weight parameters are updated by back propagation to train the Sep-RefineNet model.

4. Experimental Results and Discussion

According to the process of Figure 2, encode the potential PRI to obtain the FCM. Then, the FCM is fed into the Sep-RefineNet to achieve pixel-level classification. Finally, the intelligent deinterleaving of the radar signal is completed by position decoding. Our proposed method can accurately complete radar signal deinterleaving under 20% aliasing pulses and 20% missing pulses and has the ability to resist noise. Figure 9 is the aliasing pulses and missing pulses in the pulse stream.

4.1. Experimental Dataset

The software of generating the experimental data is Python3.7. Pytorch1.5 is used to train and predict the model, and GPU is RTX3090. We summarize the experimental data on the specific parameters of 15 radar emitters in Table 1.

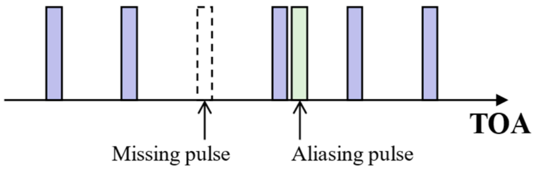

Figure 9. Radar pulse stream in presence of aliasing pulse and missing pulse.

Table 1. Fifteen radar emitter signal working parameter.

Radar Number	Intrapulse Modulation	PRI Modulation Mode	Radio Frequency (GHz)	Pulse Width (μs)	Pulse Missing Rate	Pulse Aliasing Rate	TOA Measurement Error (μs)
1	PSK	Constant	1.213~1.472	0.42~0.45	10%	10%	±5
2	LFM	Staggered	2.524~2.763	1.12~1.18	20%	10%	±5
3	LFM	Constant	2.427~2.663	1.16~1.21	15%	15%	±5
4	NLFM	Constant	0.726~0.919	0.56~0.62	20%	10%	±5
5	PSK	Jittered	1.857~2.137	0.49~0.53	5%	5%	±5
6	FSK	Jittered	2.618~2.903	0.47~0.51	10%	5%	±5
7	FSK	Staggered	0.625~0.745	0.70~0.75	15%	15%	±5
8	NS	Staggered	2.175~2.352	0.88~0.93	20%	5%	±5
9	LFM	Constant	1.211~1.477	0.92~0.97	20%	20%	±5
10	LFM	Constant	1.154~1.338	0.33~0.39	20%	15%	±5
11	FSK	Constant	0.972~1.315	1.12~1.18	20%	5%	±5
12	NLFM	Jittered	1.201~1.678	0.52~0.58	10%	20%	±5
13	NS	Staggered	2.235~2.516	0.81~0.85	15%	20%	±5
14	LFM	Jittered	1.783~2.154	0.63~0.69	15%	15%	±5
15	LFM	Constant	2.312~2.613	0.40~0.49	5%	10%	±5

The experimental data include 15 radar emitter signals, and the intrapulse modulation methods include normal signals, linear frequency modulation signals, nonlinear frequency modulation signals, etc. It includes different pulse widths and radio frequency ranges, different interference rates of aliasing pulses and missing pulses, and measurement errors. The missing pulse is a random miss that obeys the uniform distribution, and the aliasing pulse is a uniform random distribution from the initial TOA to the end TOA. The TOA measurement error conforms to normal distribution with an average value of 0 and a standard deviation value of $\sigma = 2.5$ μs. If the maximum value of the TOA measurement error exceeds twice σ, it is set equal to 2σ.

The modulation types of PRI are constant PRI, staggered PRI, and jittered PRI. The working parameters of PRI are shown in Table 2. The value of PRI is $[100,\ 500]$ and obeys the uniform distribution. The jitter error of the constant PRI does not exceed 1%. The number of sub-periods of the staggered PRI is set as $N_i = 3$ or $N_i = 4$. The jitter range of the jittered PRI $\delta \in [5\%, 25\%]$, where the jitter rate δ conforms to normal distribution with an average value of 0.15 and a standard deviation value of $\sigma = 0.05$, if $\delta < 0.05$, then $\delta = 0.05$, and if $\delta > 0.25$, then $\delta = 0.25$.

Table 2. Working parameters of different PRI modulation modes.

PRI Modulation Mode	Parameters Range
Constant PRI	$PRI \in [100, 500]$ μs, the jittered error <1%
Staggered PRI	$PRI \in [100, 500]$ μs, the number of stagger $N_i = 3$ or $N_i = 4$
Jittered PRI	$PRI \in [100, 500]$ μs, the jittered error range $\delta \in [5\%, 25\%]$

The dataset is the 15 radar emitter signals in Table 1. Randomly select 2–4 radar pulses and match them with different PRI modulation modes and working parameters in Table 2 to generate a total of 2000 aliased pulse streams. Use 80% of the experimental data for training, 10% for validation, and 10% for testing. Evaluation indicators are divided into pixel accuracy, which evaluates the fitting ability of the semantic segmentation network. Another evaluation indicator is F1-Score, which represents the ability of signal deinterleaving.

4.2. Experimental Results

The encoded FCM and paired label matrix are fed to the Sep-RefineNet for training to complete the deinterleaving of the radar emitter signals.

4.2.1. Verify the Effectiveness of Sep-RefineNet

In order to evaluate the ability of feature extraction of Sep-RefineNet and the fitting of the network, the prediction results of the FCM are compared and analyzed. The evaluating indicator is pixel accuracy, which is used to compare each element predicted in FCM with the elements in the label matrix. It can intuitively reflect Sep-RefineNet's ability to fit the FCM. The pixel accuracy is in Equation (12).

$$Pixel\ accuracy = \frac{\sum_{i=0}^{k} p_{ii}}{\sum_{i=0}^{k} \sum_{j=0}^{k} p_{ij}} \tag{12}$$

where the numerator of Equation (12) is correctly predicted pixel elements, and the denominator is all predicted pixels. Since FCM has upper triangular redundancy during encoding, only the labeled pixels are considered in the evaluation, and the background pixels are not considered. To verify the ability of learning FCM features for the proposed Sep-RefineNet, select 20 aliased pulse streams from the test set and input them into the trained Sep-RefineNet, and calculate their pixel accuracy. The test results are shown in Table 3.

Table 3. Pixel accuracy of 20 pulse streams.

Pulse stream number	**1**	**2**	**3**	**4**	**5**	**6**	**7**	**8**	**9**	**10**
Pixel accuracy (%)	97.52	97.44	95.73	97.29	98.96	97.91	98.42	96.90	95.27	97.32
Pulse stream number	**11**	**12**	**13**	**14**	**15**	**16**	**17**	**18**	**19**	**20**
Pixel accuracy (%)	98.89	97.57	99.04	96.13	98.65	99.54	96.89	98.58	97.39	96.60

Table 3 shows that the proposed Sep-RefineNet can well fit the FCM, and the average pixel accuracy of 20 aliased pulse streams is 97.60%. The image, label, and prediction results of the FCM are shown in Figure 10.

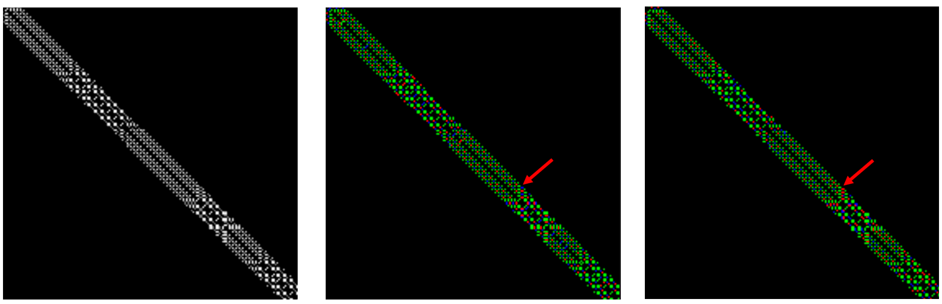

(**a**) FCM visualization (**b**) Label matrix (**c**) Prediction result

Figure 10. The partial enlargement of the FCM results for the test data: (**a**) FCM after pulse stream coding; (**b**) paired label matrix; (**c**) prediction result of FCM. The red arrow is the difference between label matrix and prediction result.

From the overall view of Figure 10b,c, Sep-RefineNet can well fit the texture, shape, and structural features of FCM. However, from the details, the direction of the red arrow is the interval between the red and blue dots in the label matrix (b), but it is four red dots connected in the prediction result (c). This could lead to the wrong sorting of the two pulses. However, according to the decoding process in Section 3.1, only the prediction results are symmetric about the diagonal of FCM and will complete the position decoding. The symmetrical position of the red arrow in the prediction matrix is not four connected red dots, which to some extent avoids the wrong sorting of the pulse signal due to the deviation of the prediction result. It improves the accuracy of signal deinterleaving.

To verify the effectiveness of the Sep-Residual unit (SRU) and focal loss (FL), the original residual unit (ORU) and cross-entropy (CE) were used to replace the improvements in this paper, and the corresponding model was trained; thus, predict the 20 test pulse streams and calculate their pixel accuracy.

In the red solid line in Figure 11, when the residual block is the Sep-Residual unit and the loss function is focal loss, the model has the highest pixel accuracy, which is better than the original residual unit and cross-entropy. The SRU fuses the features on the four channels, which will make the obtained signal features richer. Different sizes of receptive fields can better obtain the overall structural features and local texture features of FCM for convolution. The reason FL is better than CE is due to the characteristics of the FCM. The semantic segmentation task in this paper is not a traditional color image, but a two-dimensional matrix obtained by encoding a one-dimensional pulse signal through FCM. This leads to the fact that fewer effective elements on the diagonal in FCM and most of the upper triangular area is background elements. The FL allows the model to pay more attention to a small number of indistinguishable samples during the training, rather than updating the loss function indiscriminately.

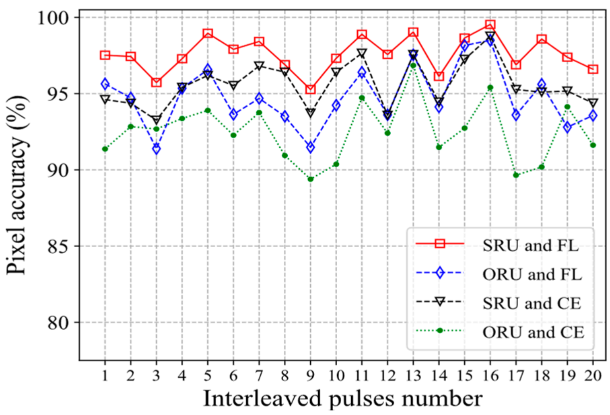

Figure 11. Comparison results of the improved Sep-residual unit and focal loss that respectively replace the original residual unit and cross entropy. The red solid line is the result of SRU and FL. Blue dotted line, black dotted line, and green dotted line are the results of ORU and FL, SRU and CE, and ORU and CE, respectively.

To verify the influence of different orders of self-correlation difference on the proposed algorithm when encoding FCM, the mean pixel accuracy and consumed time for test data of 5th order, 10th order, 15th order, and 20th order self-correlation difference were analyzed and compared in Table 4.

Table 4. Results of self-correlation difference of orders on deinterleaving.

Difference Order	5th	10th	15th	20th
Mean pixel accuracy (%)	96.51	97.60	97.66	97.14
Spend time (ms)	9.33	11.52	17.86	29.50

With the increase in the difference order in the FCM, the mean pixel accuracy is slightly improved, but the higher order will lead to a more serious harmonic influence. It leads to a decrease in deinterleaving accuracy. When reaching the 20th order, the mean pixel accuracy of the prediction results will decrease, and the mean pixel accuracy of the 15th order is 0.06% higher than that of the 10th order, but the encoding processing time of the data has increased by 55.03%. Considering that the high order will bring serious harmonics, and due to the existence of the symmetrical structure, too high order is not conducive to the decoding process. In summary, the 10th order difference is regarded as the parameter of FCM in the experiment.

To verify the effectiveness of our proposed semantic segmentation network for FCM, the Sep-RefineNet is compared with U-Net [28], Deeplab-V2 [29], RefineNet [25] and PSPNet [30]. The same data are used for training and testing.

It can be seen from Table 5 that the Sep-RefineNet has a higher mean pixel accuracy, which means that Sep-RefineNet has a better fitting ability for the FCM we built. Through multiple channels and multiple receptive fields, semantic features such as the texture and structure of FCM can be better segmented during convolution. However, the U-Net's network structure and the feature map fusion are relatively simple, and the large-scale hole convolution and pyramid hole pooling proposed in Deeplab-v2 and PSPNet for large target and background segmentation are not effective for FCM in this paper.

Table 5. The prediction results of different semantic segmentation networks.

Experimental Network	Sep-RefineNet	U-Net	Deeplab-v2	RefineNet	PSPNet
Mean pixel accuracy (%)	97.60	95.85	94.27	94.76	94.16

4.2.2. Verify the Effectiveness of Deinterleaving

The test pulse streams are fed into the network to verify the effectiveness of the proposed FCM and Sep-RefineNet for deinterleaving and are compared with traditional deinterleaving algorithms CDIF, SDIF, and PRI transformation. The threshold function of CDIF is Equation (1), and the adjustable coefficient k < 1. The threshold function of SDIF is Equation (2), and the adjustable coefficient $\alpha \in [0, 1]$ is used to control the bending and translation of the threshold curve, and k is an empirical parameter. Equations (3)–(6) are PRI transformations, which screen potential PRI according to the rules in [16]. Figure 12 is SDIF's estimation of potential PRI for different pulse streams using the same set of manual parameters α and k.

Due to the same manual threshold, parameters α and k are used in different pulse streams, the potential PRI of (b) is missed, which will lead to the missing selection in pulse sequence search. For Figure 12b, if the manual parameter k is increased and α is set appropriately so that the threshold function bends and translates downward, the missed selection of this PRI can be avoided. It reflects that the SDIF relies too much on the manual experience.

In order to evaluate the algorithm's ability of deinterleaving, recall and precision are introduced. The smaller the recall, the more serious the signal omission. The smaller the precision, the more serious the signal error sorting. The F1-Score is an indicator for the comprehensive evaluation of recall and precision. It is a comprehensive reflection of the algorithm's ability of deinterleaving signals. It is defined as follows.

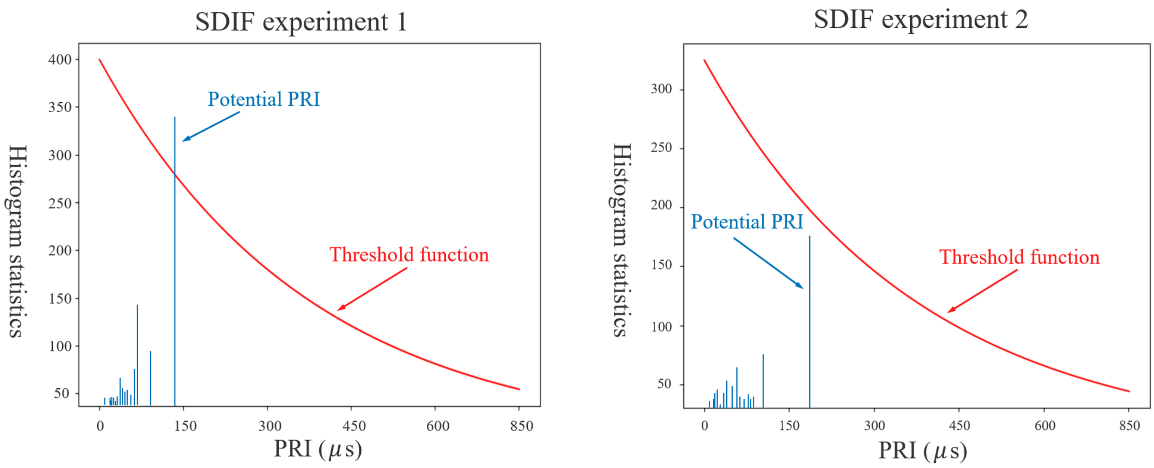

(**a**) (**b**)

Figure 12. The results of traditional SDIF algorithm sorts potential PRI. The blue line represents the potential PRI, which is estimated by the histogram statistics. The red curve represents the threshold function, and its degree of curvature and position translation are adjusted by manual parameters α and k in Equation (2). When the potential PRI exceeds the threshold function, this PRI is selected for pulse sequence search to complete signal deinterleaving. (**a**) The SDIF algorithm successfully sorts out potential PRI; (**b**) the potential PRI does not exceed the threshold, which means this potential PRI sorting failed.

$$recall = \frac{TP}{TP + FN} \tag{13}$$

$$presicion = \frac{TP}{TP + FP} \tag{14}$$

$$F1 - Score = 2 \times \frac{recall \times precision}{recall + precision} \tag{15}$$

where TP is the predicted positive sample and represents the correctly sorted pluses. FP represents positive samples that are wrongly predicted, which will lead to false alarms. FN is a negative sample of the wrong prediction, which will lead to the missed selection. Figure 13 is a comparison of the F1-Score of Sep-RefineNet and the traditional deinterleaving algorithms.

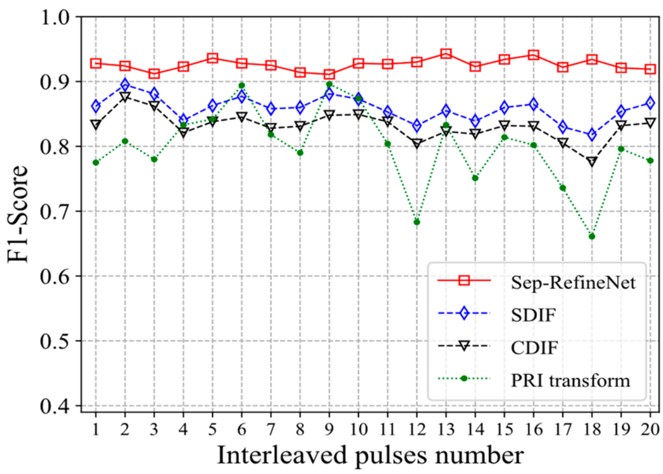

Figure 13. Comparison of Sep-RefineNet and traditional deinterleaving algorithms.

The F1-Score of the proposed method is better than traditional algorithms in terms of accuracy and stability for radar signal deinterleaving. For CDIF and SDIF, when tuning the threshold, it is necessary to estimate the pulse stream based on experience to more suitably use threshold judgment and pulse sequence search to sort pulses. In our method, after the difference order, network structure, and loss function are set in the above experiments, there is little human intervention in the deinterleaving process. PRI is encoded by FCM, then Sep-RefineNet extracts and segments the FCM, and finally completes signal deinterleaving intelligently.

4.2.3. Verify the Anti-Noise Ability

Our method is effective for different PRI modulation modes. The aliasing pulses and missing pulses are both set to 15%, and the experiments on constant PRI, staggered PRI, jittered PRI and their mixed pulses are completed. Pulse streams from the test are set to complete deinterleaving and to obtain their F1-Score. The average results are shown in Table 6.

Table 6. The F1-Score of different PRI modulation modes.

PRI Modulation Mode	Constant	Staggered	Jittered	Constant + Staggered	Constant + Jittered
F1-Score	0.982	0.885	0.872	0.933	0.917

Table 6 shows that the proposed method has an accurate sorting result for different modulation PRI. For the pulses with only constant PRI, the recall is 0.993, the precision can reach 0.971, and the F1-Score is 0.982. The sorting result of the jittered PRI will be relatively poor, but the recall rate is still 0.885, the precision is 0.859, and the F1-Score is 0.872. This is because the pulse jitter will cause the FCM to be affected during encoding, destroying the semantic features between PRI, and the jittered PRI is most affected. The reason why the recall rate is slightly higher than the precision is the position decoding is affected by the FCM difference order and the harmonics. If the Sep-RefineNet predicts the same wrong results at the symmetrical position, it will lead to error sorting, making the number of predicted pulses more than the labels. In order to verify the anti-noise ability of the proposed method, pulse streams under different interference rates were selected from the test set, and different deinterleaving algorithms were compared when the aliasing pulses and missing pulses were 5%, 10%, 15%, and 20%, respectively. The calculated F1-Score and the obtained results are shown in Table 7.

Table 7. The F1-Score under different pulse interference rates.

Aliasing and Missing Rate / F1-Score	5%	10%	15%	20%
SDIF	0.894	0.878	0.841	0.782
CDIF	0.875	0.860	0.836	0.774
PRI transform	0.836	0.814	0.753	0.683
Sep-RefineNet	0.946	0.931	0.918	0.904

Under different pulse interference rates, the proposed deinterleaving algorithm still has a good sorting effect. When the aliasing pulses and missing pulses are 5%, the F1-Score is 0.946. When the noise rate is 10%, the F1-Score is 0.931. When the noise rate is 20%, the F1-Score can still reach above 0.9. Compared with the traditional algorithm, the proposed radar signal deinterleaving algorithm is less affected by the aliasing pulses and missing pulses and has better anti-noise interference ability.

5. Conclusions

Aiming at the problems of poor anti-noise ability and over-reliance on manual parameters of traditional methods of radar signals deinterleaving, this paper proposes a method of combining encoding FCM and semantic segmentation network named Sep-RefineNet. In this paper, the FCM is used to extract the PRI features in the pulse stream, and then, the semantic segmentation method is used to identify the texture, shape, and structural features of the FCM. Finally, the deinterleaving task is completed intelligently by position decoding. Experiments show the effectiveness and anti-noise ability of the proposed method, which can accurately complete the deinterleaving, avoiding the traditional process of threshold judgment and pulse sequence search. When the aliasing pulse rate and missing pulse rate are 20%, the F1-Score of our method can still reach 0.9. The future work will consider how to increase the attention to the diagonal elements of FCM for better completion of deinterleaving. In addition, in the case of few-shot, it is possible to optimize the model and improve the practicability.

Author Contributions: Conceptualization, W.R., Z.Y., W.C., X.L. and Y.M.; investigation and analysis, X.L., W.R. and Z.Y.; software, Y.M.; validation, Y.M. and W.R.; writing—original draft preparation, Y.M. and W.R.; writing—review and editing, Y.M. All authors have read and agreed to the published version of the manuscript.

Funding: The present is funded by the National Natural Science Foundation of China (no. 62131019).

Institutional Review Board Statement: Not applicable.

Informed Consent Statement: Not applicable.

Data Availability Statement: The original contributions presented in the study are included in the article, further inquiries can be directed to the corresponding author.

Conflicts of Interest: The authors declare no conflict of interest.

Abbreviations

The abbreviations used in the manuscript are as follows:

PDW	pulse description words
PRI	pulse repetition interval
TOA	time of arrival
FCM	frequency characteristic matrix
TM	transformation matrix
Sep-RefineNet	separable refinement network
SRU	Sep-Residual unit
FL	focal loss
LR	learning rate

References

1. Gupta, M.; Hareesh, G.; Mahla, A.K. Electronic Warfare: Issues and Challenges for Emitter Classification. *Def. Sci. J.* **2011**, *61*, 228–234. [CrossRef]
2. Chen, L.; Ma, Q.; Luo, S.S.; Ye, F.J.; Cui, H.Y.; Cui, T.J. Touch-Programmable Metasurface for Various Electromagnetic Manipulations and Encryptions. *Small* **2022**, *18*, 2203871. [CrossRef] [PubMed]
3. Ma, Q.; Bai, G.D.; Jing, H.B.; Yang, C.; Li, L.; Cui, T.J. Smart Metasurface with Self-Adaptively Reprogrammable Functions. *Light Sci. Appl.* **2019**, *8*, 98. [CrossRef] [PubMed]
4. Latombe, G.; Granger, E.; Dilkes, F.A. Fast Learning of Grammar Production Probabilities in Radar Electronic Support. *IEEE Trans. Aerosp. Electron. Syst.* **2010**, *46*, 1262–1289. [CrossRef]
5. Liu, Q.; Zheng, S.; Zuo, Y.; Zhang, H.; Liu, J. Electromagnetic Environment Effects and Protection of Complex Electronic Information Systems. In Proceedings of the 2020 IEEE MTT-S International Conference on Numerical Electromagnetic and Multiphysics Modeling and Optimization (NEMO), Hangzhou, China, 7–9 December 2020; pp. 1–4.
6. Jinping, S.; Zhen, L.; Li, L.; Xiang, L. Progress in Radar Emitter Signal Deinterleaving. *J. Radars* **2022**, *11*, 418–433. [CrossRef]
7. Saperstein, S.; Campbell, J.W. Signal Recognition in a Complex Radar Environment. *Electronic* **1977**, *3*, 8.
8. Jiegui, W.; Xueming, J. Survey on deinterleaving technique for modern radar signal. *Radar Sci. Technol.* **2006**, *4*, 104–108. [CrossRef]

9. Nishiguchi, K.; Kobayashi, M. Improved Algorithm for Estimating Pulse Repetition Intervals. *IEEE Trans. Aerosp. Electron. Syst.* **2000**, *36*, 407–421. [CrossRef]
10. Kok, E.H.; Turkmen, L.E.; Unsal, S. Electronic Warfare Support Measures (ESM) Subsystem Model in a Simulated Tactical Environment. In Proceedings of the 2006 IEEE 14th Signal Processing and Communications Applications, Antalya, Turkey, 17–19 April 2006; pp. 1–4.
11. Jian, M.; Laizhao, H. Repetitive cycle transform for signal processing. *Electron. Inf. Warf. Technol.* **1998**, *13*, 1–7.
12. Mingsong, L. Research on Interpulse Parameter Sorting of Radar Signal Based on Machine Learning. Master Dissertation, Harbin Engineering University, Harbin, China, 2021. [CrossRef]
13. Mardia, H.K. New Techniques for the Deinterleaving of Repetitive Sequences. *IEE Proc. F Radar Signal Process. UK* **1989**, *136*, 149. [CrossRef]
14. Milojević, D.J.; Popović, B.M. Improved Algorithm for the Deinterleaving of Radar Pulses. *IEE Proc. F (Radar Signal Process.)* **1992**, *139*, 98–104. [CrossRef]
15. Liu, Y.; Zhang, Q. Improved Method for Deinterleaving Radar Signals and Estimating PRI Values. *IET Radar Sonar Navig.* **2018**, *12*, 506–514. [CrossRef]
16. Xin, G.; Hangping, Z. An improved algorithm PRI transform based on coherence of time delay sequence. *Radar Sci. Technol.* **2018**, *16*, 49–54. [CrossRef]
17. Wengui, Z.; Kai, L.; Jiabin, H. Sorting of the aliasing LFM radar signals based on PRI transform. *Radar Sci. Technol.* **2016**, *14*, 630–634. [CrossRef]
18. Ying, F.; Xing, W. Radar Signal Recognition Based on Modified Semi-Supervised SVM Algorithm. In Proceedings of the 2017 IEEE 2nd Advanced Information Technology, Electronic and Automation Control Conference (IAEAC), Chongqing, China, 25–26 March 2017; pp. 2336–2340.
19. Wei, S.; Qu, Q.; Su, H.; Wang, M.; Shi, J.; Hao, X. Intra-Pulse Modulation Radar Signal Recognition Based on CLDN Network. *IET Radar Sonar Navig.* **2020**, *14*, 803–810. [CrossRef]
20. Qu, Z.; Hou, C.; Hou, C.; Wang, W. Radar Signal Intra-Pulse Modulation Recognition Based on Convolutional Neural Network and Deep Q-Learning Network. *IEEE Access* **2020**, *8*, 49125–49136. [CrossRef]
21. Ning, B. Radar Signal Sorting Method Based on Neural Network. Master's Thesis, Xidian University, Xi'an, China, 2019. [CrossRef]
22. Li, X.; Liu, Z.; Huang, Z. Attention-Based Radar PRI Modulation Recognition With Recurrent Neural Networks. *IEEE Access* **2020**, *8*, 57426–57436. [CrossRef]
23. He, K.; Zhang, X.; Ren, S.; Sun, J. Deep Residual Learning for Image Recognition. In Proceedings of the 2016 IEEE Conference on Computer Vision and Pattern Recognition (CVPR), Las Vegas, NV, USA, 27–30 June 2016; pp. 770–778.
24. Santurkar, S.; Tsipras, D.; Ilyas, A.; Madry, A. How does batch normalization help optimization? *arXiv* **2019**, arXiv:1805.11604.
25. Lin, G.; Milan, A.; Shen, C.; Reid, I. RefineNet: Multi-Path Refinement Networks for High-Resolution Semantic Segmentation. In Proceedings of the 2017 IEEE Conference on Computer Vision and Pattern Recognition (CVPR), Honolulu, HI, USA, 21–26 July 2017; pp. 5168–5177.
26. Müller, R.; Kornblith, S.; Hinton, G.E. When Does Label Smoothing Help? In Proceedings of the Advances in Neural Information Processing Systems, Curran Associates, Inc., Vancouver, BC, Canada, 8–14 December 2019; Volume 32.
27. Lin, T.-Y.; Goyal, P.; Girshick, R.; He, K.; Dollár, P. Focal Loss for Dense Object Detection. *IEEE Trans. Pattern Anal. Mach. Intell.* **2020**, *42*, 318–327. [CrossRef] [PubMed]
28. Ronneberger, O.; Fischer, P.; Brox, T. U-Net: Convolutional Networks for Biomedical Image Segmentation. In Proceedings of the Medical Image Computing and Computer-Assisted Intervention–MICCAI 2015, Munich, Germany, 5–9 October 2015; Navab, N., Hornegger, J., Wells, W.M., Frangi, A.F., Eds.; Springer International Publishing: Cham, Switzerland, 2015; pp. 234–241.
29. Chen, L.-C.; Papandreou, G.; Kokkinos, I.; Murphy, K.; Yuille, A.L. DeepLab: Semantic Image Segmentation with Deep Convolutional Nets, Atrous Convolution, and Fully Connected CRFs. *IEEE Trans. Pattern Anal. Mach. Intell.* **2018**, *40*, 834–848. [CrossRef] [PubMed]
30. Zhao, H.; Shi, J.; Qi, X.; Wang, X.; Jia, J. Pyramid Scene Parsing Network. In Proceedings of the 2017 IEEE Conference on Computer Vision and Pattern Recognition (CVPR), Honolulu, HI, USA, 21–26 July 2017; pp. 6230–6239.

Disclaimer/Publisher's Note: The statements, opinions and data contained in all publications are solely those of the individual author(s) and contributor(s) and not of MDPI and/or the editor(s). MDPI and/or the editor(s) disclaim responsibility for any injury to people or property resulting from any ideas, methods, instructions or products referred to in the content.